JOURNAL OF MATERIALS SCIENCE 2 (1967) 589–609

Ion-Implantation Doping of Semiconductors

L. N. LARGE
Services Electronics Research Laboratory, Baldock, Herts, UK

R. W. BICKNELL
Allen Clark Research Centre, The Plessey Co Ltd, Caswell, Towcester, Northants, UK

Received 3 August 1967

For some time now, the bombardment of solids by heavy ions has been an active field of research. It has been carried out for a variety of reasons, for example with a view to increasing knowledge of atomic collision processes and how they relate to such phenomena as secondary electron emission and sputtering. In addition, the implantation of inert-gas ions followed by thermal treatment of the bombarded solid has been undertaken with a view to studying diffusion processes and thereby providing information on the damage induced by the bombardment. More recently, ion implantation has become important as a means of changing the electrical and chemical properties of the bombarded material. Of particular interest is the doping of semiconductors in order to produce changes in the conductivity of the material in a highly controlled manner. In this field, the technique is not merely a diagnostic tool but may well become an important addition to the present-day industrial technology of production of solid-state circuits and devices.

1. Introduction

In 1952, Ohl [1] published an account of the bombardment of silicon point-contact diodes, observing that the damage induced by ion bombardment destroyed the rectifying properties but that these could be restored by annealing. In 1955, Cussins [2] observed similar effects on germanium junctions, but it was as recently as 1960 that the first p-n junctions produced by ion bombardment were reported, by Rourke, Sheffield, and White [3]. Group III and V elements were implanted into silicon at concentrations up to 10^{18} ions/cm^3 to produce shallow p-n junctions. Later, important contributions were made by McCaldin and Widmer [4], Ferber [5], and King [6]. Since that time, the interest in this technique has slowly increased as devices become more sophisticated and demand higher degrees of control in their manufacture. In order to assess the potential of this technique, the fundamental material aspects of ion implantation are being studied, such as the penetration profiles, the electrical activity, and the effects of damage to the material with particular reference to how this can be minimised.

In the UK, work on ion-implantation doping of semiconductors was started some two years ago at SERL*, Baldock, and it was recognised that, in the field of solid-state research and technology, a very close cooperation with industry was necessary. The work at SERL has therefore been a joint project in conjunction with parts of the electronics industry. The effort has been further increased by the participation of the UKAERE† at Harwell who have worked on some aspects of ion bombardment, for example the study of damage to materials, for many years.

2. The Range of Heavy Particles in Matter

High-energy ions lose their energy as they pass

*Services Electronics Research Laboratory
†United Kingdom Atomic Energy Research Establishment

through a solid, by collision processes with both target electrons and atoms. The detailed processes involved were treated theoretically by Bohr [7] in 1948, when he showed that the most important criterion determining which of these processes was dominant was the velocity of the particle. For particles of high velocity compared with the velocity of the electron in the Bohr model of the hydrogen atom the dominant energy-loss processes are those in which energy is imparted to target electrons, so-called electronic collision processes. As the velocity is reduced, the dominant process becomes that in which energy is imparted to individual target atoms, so-called nuclear collision processes. In the latter case, the collision process may be elastic in nature, and the struck atom may be displaced from its position in the lattice with sufficient energy itself to displace many others. The velocity above or below which each of these processes dominates is not in fact discrete, as postulated by Bohr. Later developments of the theory by Lindhard, Scharff, and Schiott [8] (referred to below as LSS) show that, at velocities considerably below that of the electron in the Bohr atom, electronic excitation and ionisation can take place and must be taken into account when computing the theoretical range of particles. The results of the LSS theory for heavy particles bombarding a random collection of target atoms (e.g. an amorphous solid) show that the incident particles come to rest in an approximately Gaussian distribution about a mean range. They derive a universal range/energy plot which is a function of the atomic numbers and masses of the impinging and target atoms, the number of stopping atoms per unit volume, and the incident particle energy. A number of curves are produced for different values of a constant, known as the electronic stopping constant, which is itself a function of the incident and struck atom masses and which increases as the role of electronic collision processes becomes more significant. In the nuclear collisions, the incident ions may be scattered through a considerable angle if the mass of the incident ion is smaller than that of the target material. The range derived theoretically is that measured along the direction of the path of the particle, so that a correction has to be applied if the penetration depth from the surface is required. This "projected range" is also available from LSS theory. The following important points emerge from the range/energy theory. (*a*) When electronic processes dominate in the energy loss mechanisms, the mean range may be considerably greater than the Gaussian half-width, whereas the range when nuclear collision processes predominate is often comparable with the half-width. Figs. 1 and 2 illustrate this point. (*b*) For a given combination of incident atom and struck atom, the Gaussian half-width increases with increasing range and therefore with increasing incident particle energy.

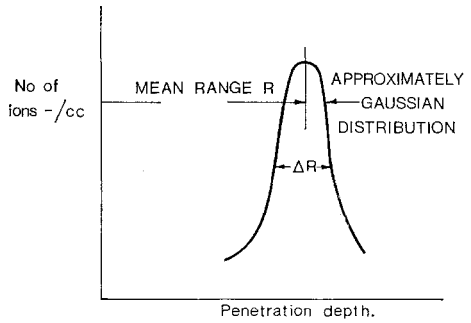

Figure 1 Distribution of ions from a bombardment when electronic collision processes predominate.

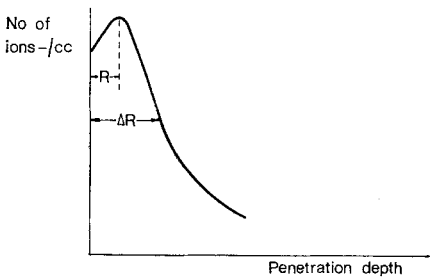

Figure 2 Distribution of ions from a bombardment when nuclear collision processes predominate.

3. Channelling of Heavy Ions

Up to this point, the interaction of ion beams with amorphous solids only has been considered, and some of the resulting distributions indicated. When single crystals are used as targets, the distribution of stopped ions as a function of depth may be considerably modified, since a fraction of the bombarding particles may travel between planes or rows of atoms so that no close atom collisions take place. This phenomenon is known as "channelling" and results in a fraction of the ions penetrating to a much greater range in the crystal than in an amorphous solid of similar atom density. Experiments by Davies and his coworkers [9,10] showed the existence of penetrating "tails" on the particle distributions

when crystalline materials were bombarded. In 1963, Robinson and Oen [11] published computer studies in which channelling was predicted. Since that time, channelling has been studied in more detail, but a great deal of work still needs to be done to understand and control this phenomenon. The beam of particles may be deliberately aligned with "open" crystal directions (e.g. ⟨1 1 0⟩ directions for the diamond structure), and the modification to the Gaussian distribution may be typically as shown in fig. 3. If the beam

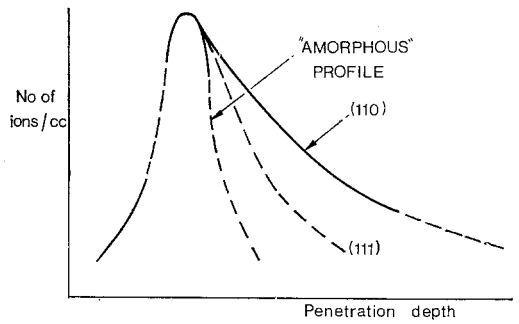

Figure 3 Modification of Gaussian distribution when channelling occurs in single-crystal targets.

collimation is particularly good, and low doses are used, it is possible to produce a much larger fraction of channelled particles, so that the resulting distribution may be as obtained by Dearnaley [12] and shown in fig. 4. With the practical existence of large-scale crystal defects, it is difficult to predict the channelled profiles theoretically, so that quantitative data for the penetration depth in crystalline solids is for the most part experimental.

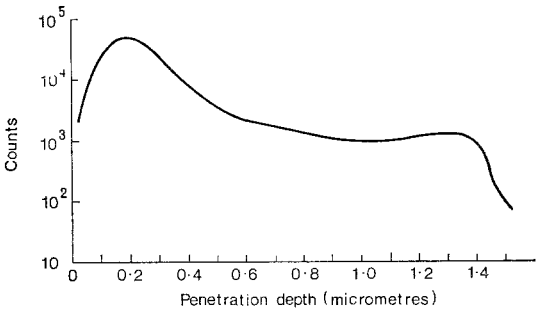

Figure 4 Channelling by 110 keV P^{32} ions with dose of $1.5 \times 10^{13}/cm^2$ <1 1 0> orientation.

Interesting aspects of channelling for materials study are that channelled particles cause very little or no damage to the solid through which they are travelling and in some respects are similar to interstitial diffusers. Those particles which collide with host atoms nearer the surface, however, can displace atoms from their sites and block the channels, so that, in order to control the process, it is necessary not only to orientate the crystal accurately with respect to the ion beam but also to prevent blocking occurring, by heating the crystal during bombardment.

4. Apparatus Used in Ion Implantation

The basic requirements are: (i) a source of ions; (ii) a means of accelerating these ions; (iii) mass analysis of the beam; and (iv) a suitable target chamber in which the bombarded material is mounted. The crystal must be capable of accurate alignment with respect to the beam. Figs. 5a, 5b, and 5c show typical apparatus in use at

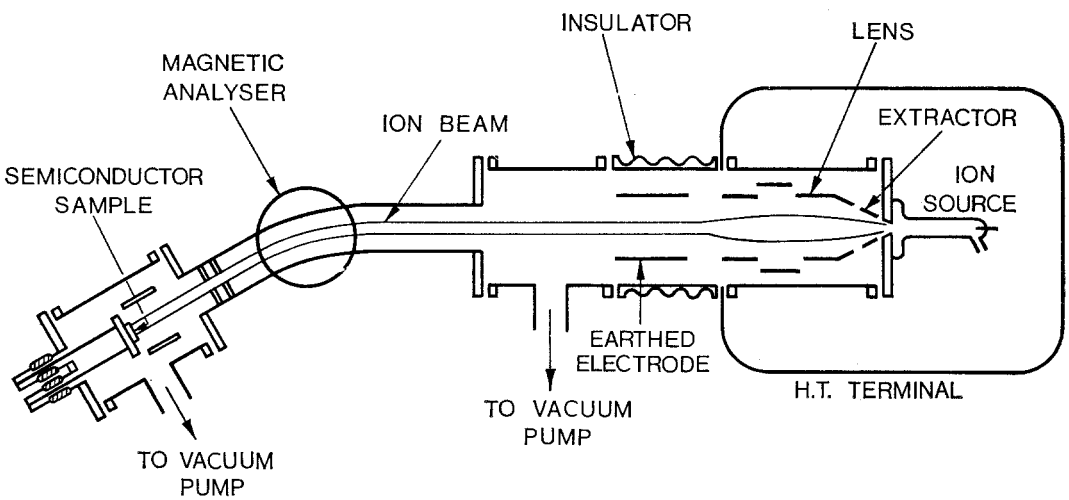

Figure 5a Schematic diagram of ion-implantation apparatus.

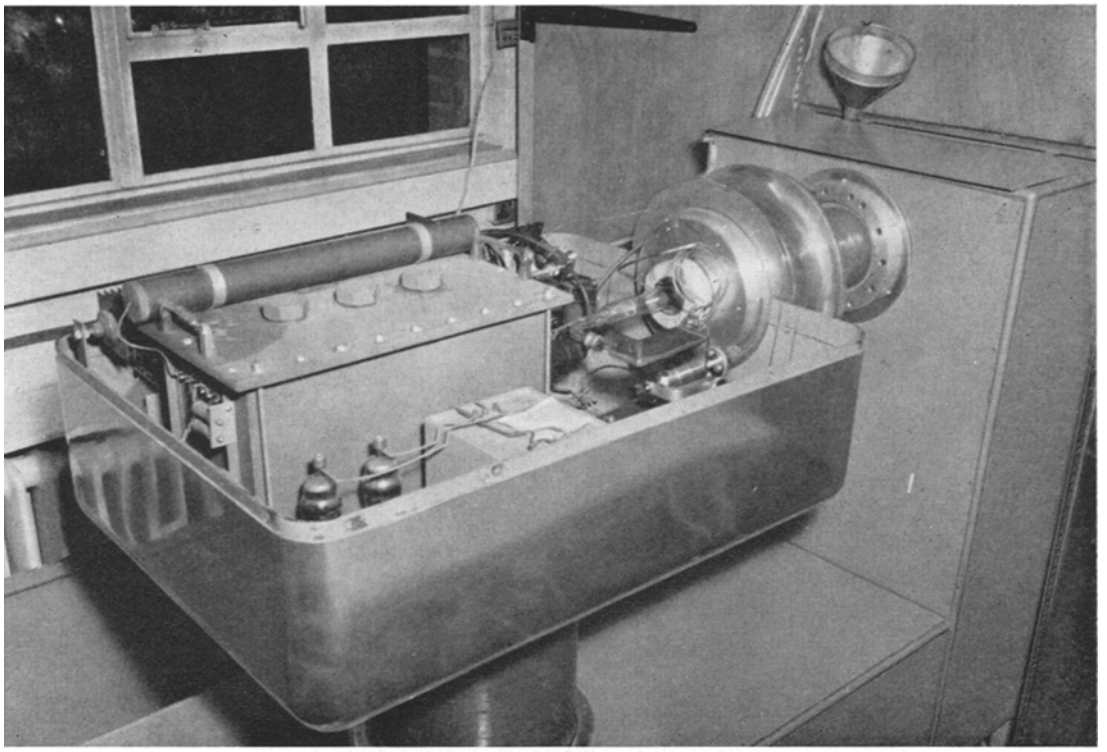

(b)

(c)

Figures 5b and 5c Typical apparatus in use at SERL.

SERL. An r.f. ion source is used in which a compound of the gas such as phosphorus trichloride is maintained at a pressure between 10^{-2} and 5×10^{-2} torr. The r.f. field applied produces an ionised plasma and this is enriched by the application of an axial magnetic field causing the electrons in the ion source to take helical paths, thereby increasing their ionisation. The ions are extracted through a small canal which also provides a means for differentially pumping the accelerator tube (at $\sim 10^{-6}$ torr) with respect to the ion source bottle. The r.f. ion source is maintained at high potential with respect to earth by enclosing it and all relevant power supplies in a metal container suitably insulated from earth and deriving its own potential by a separate electrostatic generator. The positive ions, after extraction through the canal, are focused and accelerated to earth potential, then they are mass-analysed to select a particular species. This is then allowed to impinge on the crystal surface in the target chamber. A system of electrodes surrounding the specimen to be bombarded provides for suppression of the secondary electrons emitted from the target surface. This allows a very accurate measure of the total charge injected by monitoring the target current and time of bombardment, so that the amount of dope implanted is known accurately. Typical apparatus in use at SERL will operate at voltages up to 150 kV and provide beams of boron, phosphorus, and many other ions suitable for doping. An important feature of such apparatus is the pressure of background gases during bombardment. This has been kept to a minimum by using vac-ion pumps on the target chamber, and traps on the backing lines of any diffusion pump elsewhere. This avoids, for example, contamination of the target surfaces by "cracking out" of carbon from organic gases. All samples are mounted in a clean bench before loading into the target chamber. During ion implantation, the presence of dust on the surface of a crystal causes shadowing of the beam and, owing to the well-defined directional properties of fast ions, it is possible to produce undoped "pipes", which can have serious consequences in semiconductor work.

With the machine described, it is easy to obtain ~ 1 μA of boron or phosphorus ions, which means that an area of 1 cm^2 of crystal can be doped uniformly to a depth of 0.5 μm and doping level of 10^{19}/cm^3 by using a total charge of 80 μC or 1 μA of beam current for 80 sec. The ion current could be increased to 10 μA or more on a machine designed for industrial use, permitting a larger number of samples to be doped in a given time. There are many alternative types of ion source that can be used for ion implantation and some of these will provide a large number of ion species. The r.f. ion source is extremely simple, rugged, and capable of long life even with the corrosive compounds employed.

5. Radiation Damage and Material Effects

The study of damage induced in semiconductor material by ion implantation is of great importance in ascertaining the usefulness of the technique, and for this reason the results to-date are treated in some detail in this article. There is little published work, however, on damage in silicon, and a joint programme between SERL and The Plessey Co Ltd at Caswell is being carried out, with samples irradiated at SERL being examined by Plessey.

The results discussed here are in the main those obtained in this programme, except where other workers are specifically referred to: for example. radiation damage effects have been the subject of detailed studies at the UKAERE, and reference is made to a number of their results.

The examination of ion-beam damage in single-crystal semiconductors presents problems because of the small scale of the damage which occurs [13]. It is best examined by using electron diffraction and electron microscopy methods. Apart from glancing-angle electron diffraction, transmission electron microscopy and diffraction methods are used; but, because of the high absorption of electrons in solids, examination is limited to thicknesses of less than 1 μm or, for high-resolution microscopy, less than 0.1 μm. Several methods of suitably thinning specimens for electron microscopy are available, but the semiconductors silicon and germanium are best thinned by etching, a method which does not introduce work damage. Since damaged and faulted material dissolves more readily than undamaged material [14], it is usual to prepare suitable specimens for the electron microscope before ion implantation. A typical procedure is to drill ultrasonically discs 2.2 mm in diameter from (1 1 1) silicon slices about 100 μm thick (2.2 mm diameter is suitable for insertion into electron-microscope grid holders). After cleaning, the discs are then waxed face down over a hole in

thin PTFE* sheet, and the exposed back surface of the disc is jet-etched [15] with 1:9 HF/HNO_3 acid solution until a small straw-coloured patch is visible by transmitted light in the centre of the disc (fig. 6). The etching rate can then be slowed

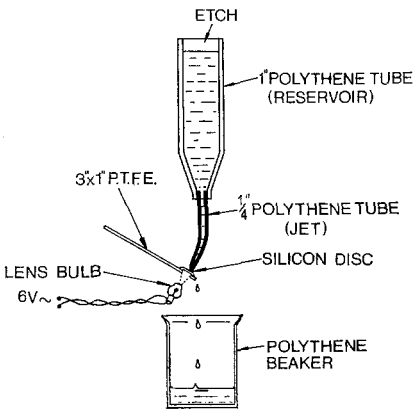

Figure 6 General arrangement of jet thinning apparatus. The etch is dripped onto the silicon at about 5 cm^3/min until straw-coloured hole is visible by transmission.

by diluting the etch with water. This technique gives areas of about 0.1 mm diameter of suitable thickness for electron microscopy often with areas of tapered thickness around holes where etch pits have broken right through (see figs. 7 and 8).

Nearly all detail in electron microscopy of thin single crystals is contrast due to diffraction [16], and it is very sensitive to the orientation of the specimen. To ensure that observed effects may be reasonably attributed to bombardment, and not to artifacts introduced by specimen orientation and preparation, it is necessary to provide neighbouring areas of bombarded and unbombarded material for simultaneous comparison. This may be achieved by bombarding the specimen, masked with a copper electron-microscope grid, placed in contact with the front surface [17]. The bars of the grid are sufficiently thick to prevent ions reaching the surface of the silicon except in the unmasked areas, and they provide a sharp cut-off between the bombarded and umbombarded areas (figs. 7 and 8), which can be examined simultaneously at the same angle of orientation.

The observed effects of ion-bombardment damage are fairly general and, although the effects of bombarding with a heavy ion are more pronounced, silicon bombarded with boron

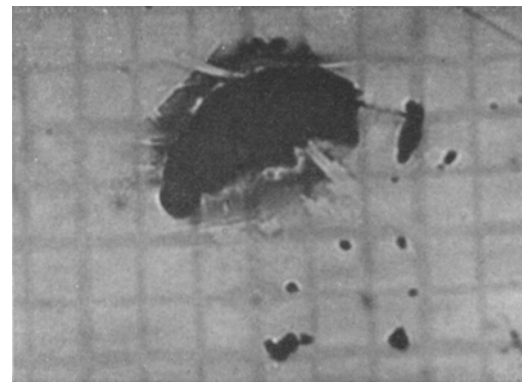

Figure 7 Optical micrograph of silicon disc implanted with 4×10^{15} (at. wt 35) ions/cm^2. The grid pattern indicates the unbombarded areas shielded by the 200-mesh copper electron-microscope specimen grid. The dark holes are etched through pits. ($\times$ 60)

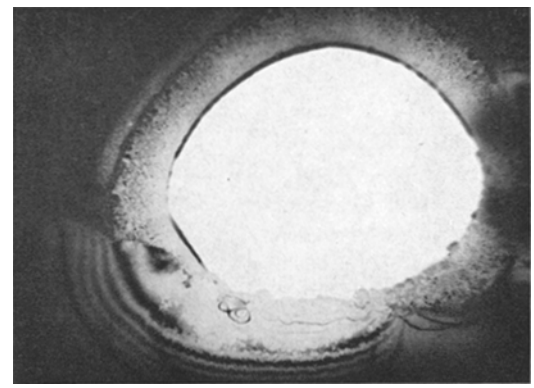

Figure 8 Electron micrograph of an etch pit in the specimen shown in fig. 7, after anneal. The thickness fringes at the bottom are in the unbombarded area and the light-coloured area round the etch pit is polycrystalline silicon. ($\times$2200)

ions gives typical results. The damage first visible by microscopy in bombarded silicon is the gradual decrease in the contrast of extinction contours as shown in fig. 9 and also reported by Parsons [13]. This is accompanied in the diffraction pattern by the appearance of diffuse haloes or rings surrounding the central spot (fig. 10). The visibility of both effects depends upon ion dose, type, and specimen thickness, but with silicon less than 0.01 μm thick the extinction contours have disappeared, and the diffraction pattern consists only of diffuse haloes when the ion dose has reached 10^{16}/cm^2 for boron. The lower limit at which boron ion damage has been observed in silicon at

*polytetrafluoroethylene

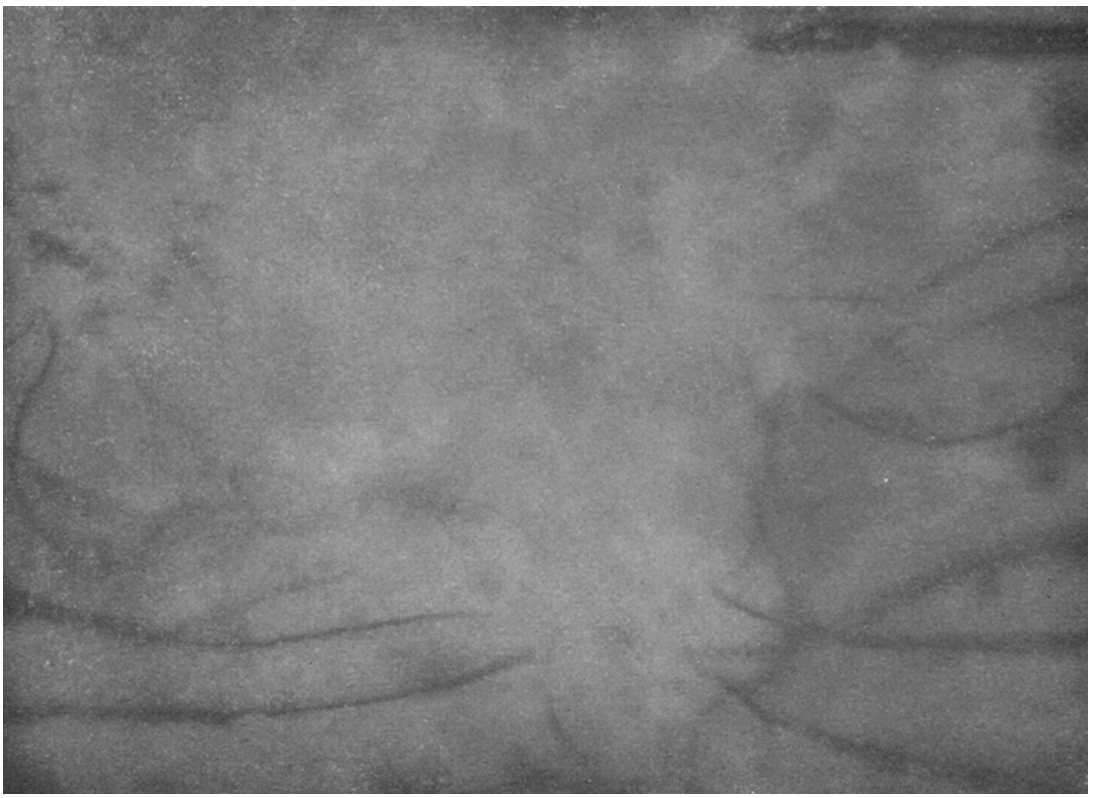

Figure 9 Electron micrograph of the specimen in fig. 7 before anneal. The bottom of the triangular-shaped etch pit without diffraction contours is completely amorphous. (× 46 000)

Caswell is $\sim 10^{14}$ boron ions/cm^2; although there have been reports of visible damage at much lower doses (e.g. 10^{12} oxygen ions/cm^2) in germanium reported by Parsons [13]. At this level, the diffraction haloes are only just detectable, and, in microscopy, small volumes less than 100 Å in diameter having different contrast from the bulk material have sometimes been observed [13]. When thicker areas of heavily bombarded silicon are observed, it is apparent that the damaged layer is confined to the front bombarded surface. Strong spots in the diffraction pattern from the undamaged silicon are circled by diffuse haloes from the damaged layer (fig. 11) – a double diffraction effect, whereby the spots from the single-crystal diffraction pattern act as sources for diffraction by the damaged material, or vice versa, depending on whether the specimen is examined with the undamaged silicon uppermost or below in the microscope. Even thicker areas of silicon will give a strong Kikuchi pattern in diffraction, but there is an increase in the diffuse background.

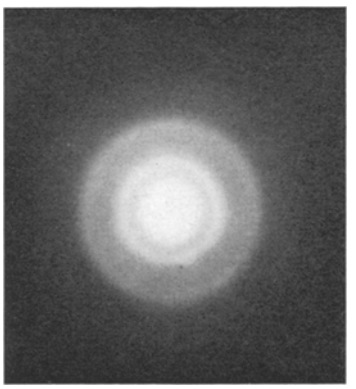

Figure 10 Amorphous halo diffraction pattern from an area such as that shown in the centre of fig. 9.

Photometer traces of the diffraction plates show a very steeply falling background intensity modulated by the diffraction haloes around the centre spot (fig. 12). This is typical of non-crystalline diffraction, and, to obtain information about the atomic packing arrangement that leads to the diffraction, a Fourier transform must be

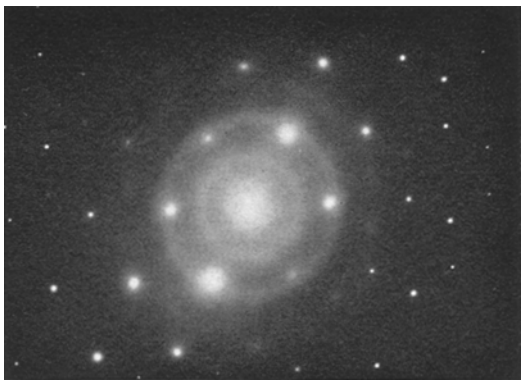

Figure 11 Double diffraction pattern from an amorphous silicon layer on top of undamaged silicon.

calculated from the diffracted intensities [18]. It is beyond the scope of this article to discuss either the method of calculation or the detailed analysis of the resulting radial distribution curve [18]. A typical radial distribution curve from ion-bombarded silicon is shown in fig. 13, and the very strong peak at 2.35 Å corresponds to the first nearest-neighbour interatomic distance found in crystalline silicon. The second peak at 3.85 Å is broader, indicating a variation in bond length of second nearest neighbours, but subsequent peaks do not correlate with the expected peak heights that would be found in crystalline silicon (table I). The results are very similar to those obtained by Richter and Breitling for amorphous silicon [19] and it must be inferred that, although the silicon is still tetrahedrally bonded, a large degree of rotation of the bonds is allowed, and the second nearest-neighbour distances are blurred. There is also the indication that third nearest neighbours at 4.48 Å are practically missing. Since (in fig. 13) there are no large resolved peaks at distances greater than 6 Å, the structure may either be regarded as an average material at distances greater than this, or it is possible that the silicon exists as small crystalline particles of about 6 Å radius. In the latter case, the resulting large number of surface atoms, possibly with incomplete bonding, would explain the ease with which the surface of ion-bombarded silicon is dissolved in aqueous HF.

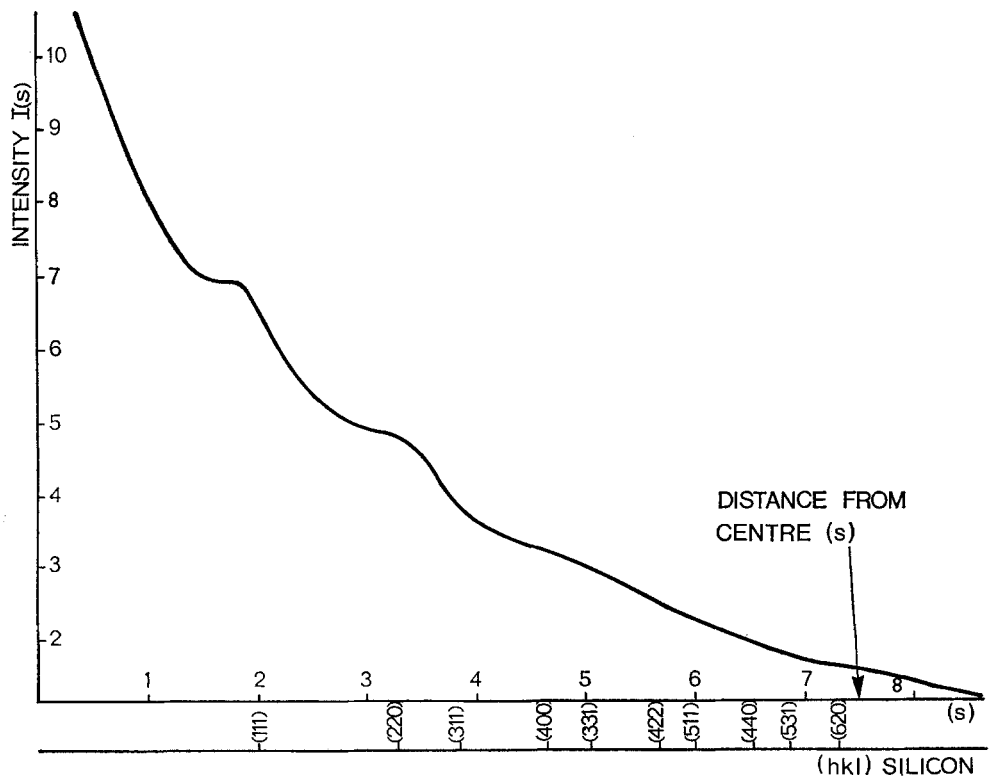

Figure 12 Photometer trace of the amorphous ring patterns in fig. 10. $I(s)$ is the relative scattered intensity at s, where $s = (4\pi/\lambda)\sin\theta$ and θ is the scattering angle. The (h k l) values show the s values at which rings from polycrystalline silicon would occur.

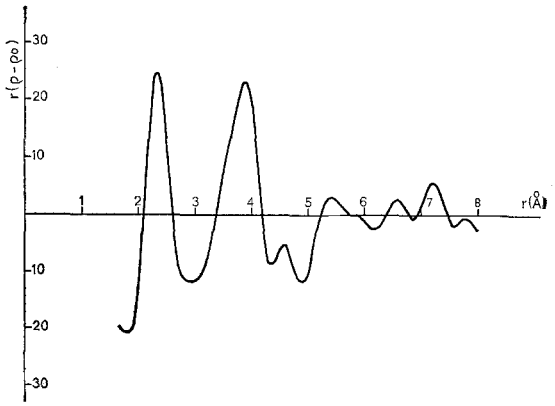

Figure 13 Radial distribution curve obtained from the scattering curve shown in fig. 12. Peaks on this curve correspond to $r\rho$, where ρ is the electron scattering density at radius r.

It has been noted by us and others, [14] that the non-crystalline layer which is completely removed in aqueous HF is an order of magnitude thinner than the expected penetration distance of the bombarding ions. This is an indication that the energy transfer in the primary collisions is only sufficient to cause displacements amongst the silicon atoms in the surface layer, and, as might be expected, the momentum transfer and hence the damage is greater when heavier ions are used.

In order to reduce radiation damage and to allow the interstitial boron atoms to "go substitutional", ion-implanted silicon is annealed at relatively low temperatures (600 to 800° C for $\frac{1}{2}$ h is typical). The structural effects of similar anneals on ion-implanted semiconductor electron-microscope samples have been studied. All observers agree that the diffuse diffraction rings disappear and that the material regains its crystallinity. There are, however, many residual defects in the layer which has been bombarded,

Figure 14a Enlarged micrograph of the area of bombarded and annealed silicon shown in fig. 8. The unbombarded silicon at the bottom of the picture contains no defects; the thin area at the top right has become polycrystalline; whilst the amorphous silicon overlying the undamaged silicon (top left) has recrystallised epitaxially, but contains many dislocation loops (× 46 000).

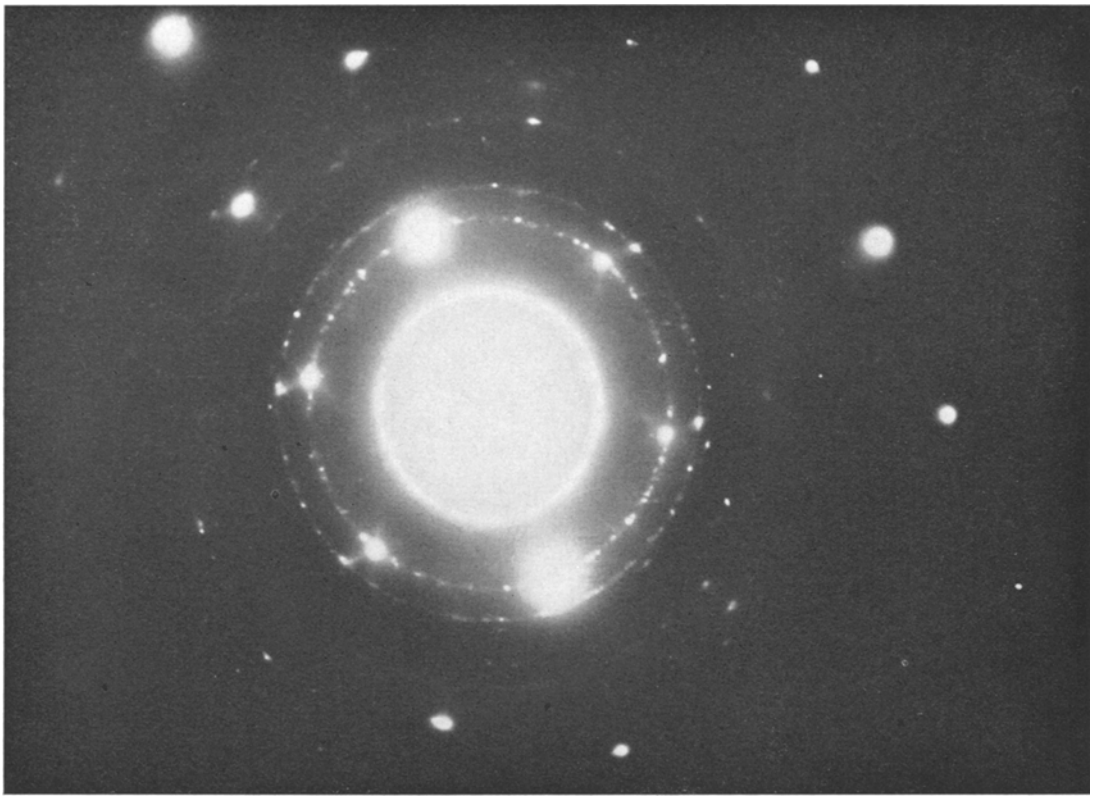

Figure 14b Diffraction pattern from the polycrystalline area of silicon at the top right of fig. 14a.

TABLE I Interatomic distances and number of atoms *N* in Silicon.

Crystalline silicon	r(Å)	2.35	3.83	4.48	5.42	5.91	6.63	7.05	7.66
	N	(4)	(12)	(12)	(4)	(12)	(24)	(16)	(12)
Damaged silicon	r(Å)	2.35	3.85	4.6	5.4	5.9	6.6	7.2	7.8
Estimated	*N*	(4)	(13)	(2)	(8)	(3)	(7)	(6)	(5)

which depend to a large extent on the type and degree of implantation and annealing schedule. On thinned silicon specimens which have been heavily bombarded, e.g. 4×10^{15} (at. wt 35) ions/cm^2, the thinnest areas, which are rendered completely non-crystalline throughout their thickness, become random polycrystalline areas with annealing, as shown in figs. 14a and 14b, the crystal size growing to about 250 Å. Neighbouring areas which are completely non-crystalline, but which overlie crystalline silicon, recrystallise epitaxially with the layer underneath. They sometimes, however, contain twin material, especially if (1 1 1) silicon slices are examined. A typical example of this is shown in fig. 15. Beneath these heavily bombarded areas, there is always a high density of dislocation loops. These are predominantly of two types, some approximately circular (fig. 16a), and others which form very long narrow dipoles as shown in fig. 16c. The type and size of loop is very variable, heavy bombardment (10^{16} ions/cm^2) and lower temperature anneals (700° C/1 h) tend to produce more and smaller loops (figs. 16a, 17a) than lower doses (10^{15} ions/cm^2) and higher temperature anneals (800° C/1 h), which produce larger loops and dipoles (fig. 16c). Both types of loops are often accompanied by long straight dislocations (fig. 16b). The depth of these defects below the surface has only recently been determined by the authors, in experiments by which the bombarded and annealed silicon was repeatedly anodised to 100 V in a phosphoric acid/amyl alcohol

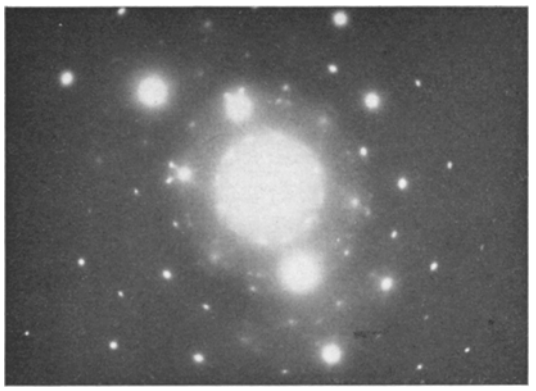

Figure 15 Diffraction pattern showing the large amount of twinning which occurs when the amorphous ion-implanted silicon later recrystallises epitaxially with the undamaged silicon beneath it.

electrolyte, and the resulting silicon oxide was removed in aqueous HF solution. Specimens thinned by this method showed that the condensed defect in silicon, bombarded with 25 and 50 keV boron ions lay in the top 2500 Å. The loops were nearest to the surface, and the long straight dislocations were the last to disappear on thinning (figs. 17a, 17b, 17c).

It is also known that the defects do not occur in the thinner areas of the specimen around holes, and, although it is possible that migration during annealing may enable them to escape to the surface, it is much more probable that the thin areas are much too close to the top bombarded surface to contain a sufficient concentration of interstitials and vacancies to condense into loops. This can be seen in fig. 18, where the thin areas near to the edge of the etch pit are free from loops.

In silicon bombarded with neon ions, Mazey *et al* [17] have observed the loops to be decorated with neon bubbles, and they concluded that the loops were near the ends of the range of neon ions (i.e. in the relatively undamaged silicon below the surface layer). The loops can be of either vacancy or interstitial type [20] and may be

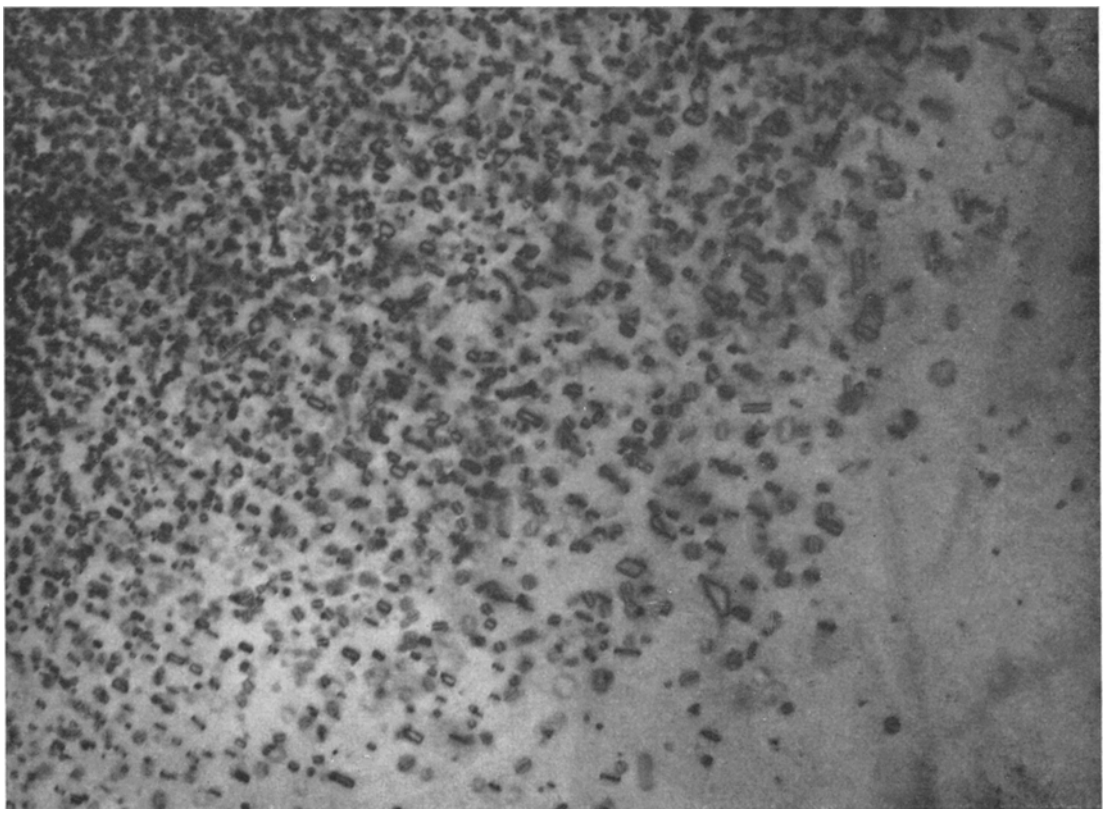

Figure 16a Electron micrograph showing the large number of small loops which occur in annealed, heavily bombarded silicon (dose 4×10^{15} boron ions/cm^2), annealed 800°C/$\frac{1}{2}$h. ($\times$ 46 000)

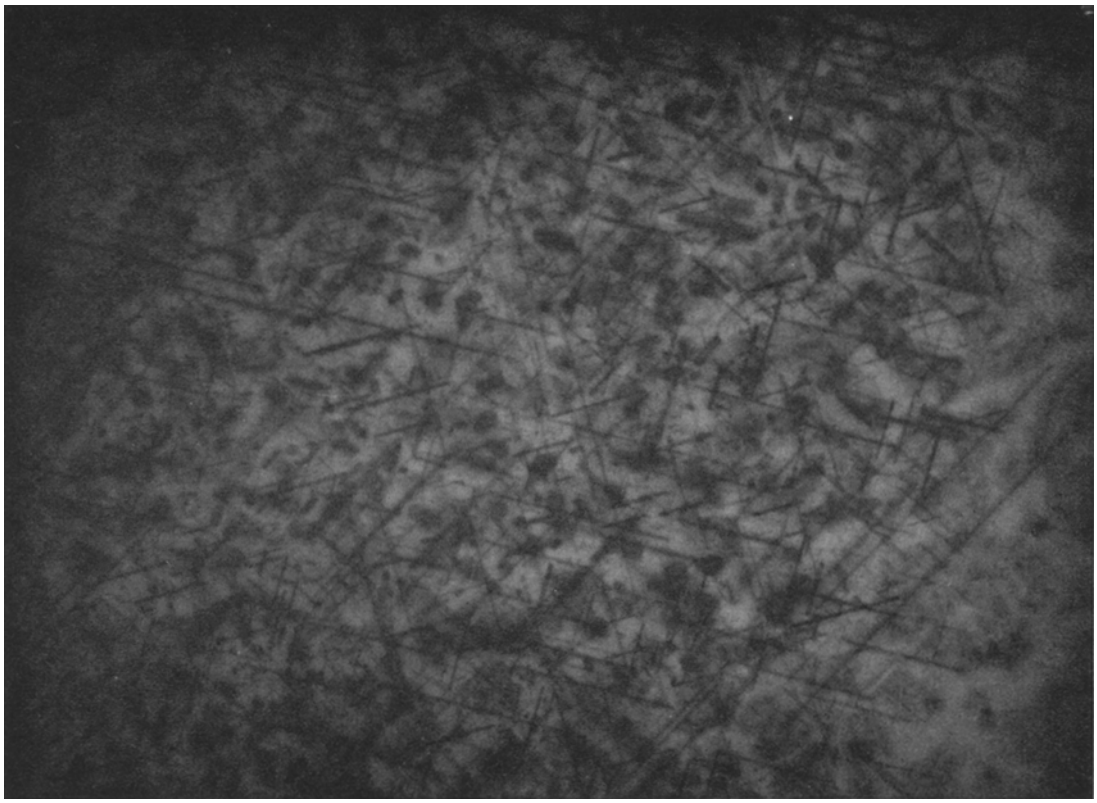

Figure 16b Electron micrograph showing dislocation loops and long straight dislocations in annealed, heavily bombarded silicon (dose 4 × 10^{15} boron ions/cm^2), annealed in microscope at ~ 800° C (× 46 000).

considered as a disc of close-packed atoms either removed or inserted into the regular crystal lattice, the resultant strain being taken up round the periphery of the loop by a series of dislocations. By using a specimen-tilting goniometer stage in the microscope, it is possible to tilt the dislocations in and out of contrast. By so doing, the dislocation vectors can be determined by a method outlined by Hirsch *et al* [21]. It is then possible to say if the loops are of interstitial or vacancy type. There are no indications from SERL irradiated specimens examined at Caswell that there is a predominance of any one type, although insufficient have been analysed to be conclusive. Another type of defect which can give very similar diffraction results to small dislocation loops is the strain occurring around precipitates in a crystal, as reported by Ashby and Brown [22]. These may be confused with dislocation loops and care must be taken to refer to the solubility limits of the implanted ions when interpreting results.

The effects of bombardment and annealing have been observed to a lesser extent by glancing-angle diffraction. In this case, it is not necessary to prepare the specimen specially, and large flat areas are quite suitable. The reduction of the surface to a non-crystalline state is readily observed, and also the production of a twinned epitaxial layer upon annealing such a surface [23]. The degree of twin formation is, of course, influenced by the substrate orientation, there being a much greater chance of twin formation in (1 1 1) layers than in other orientations, owing to the relative ease of double position twinning about the (1 1 1) normal. It has not yet been possible to determine by electron microscopy the effect on crystal damage by channelling. However, the optical reflectivity of silicon is altered by ion-beam damage, as reported by Nelson *et al* [24], and photographs as a paler shade than unbombarded areas. In the experiment reported by Nelson *et al*, in which silicon was bombarded at varying angles to the surface around the speci-

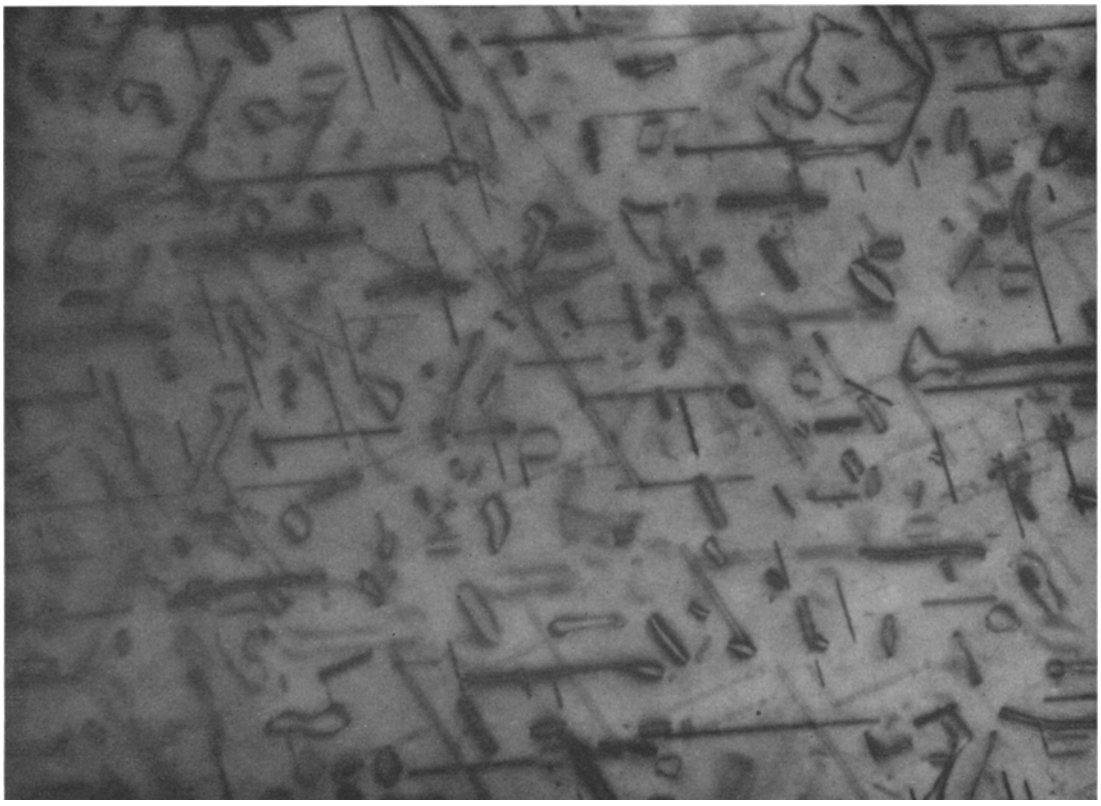

Figure 16c Electron micrograph showing elongated loops and dipoles in annealed, heavily bombarded silicon (dose 4×10^{15} boron ions/cm^2), annealed in microscope at over 800° C (× 46 000).

men normal by 80 keV neon ions, the major crystallographic directions of the silicon are delineated by regions of higher reflectivity, showing that the surface damage is very much reduced when the ions are incident in the major channelling directions. Figs. 19a and 19b show the results obtained by these workers.

6. Effect of Annealing Temperature on Conductivity of Doped Layers

There is, as yet, little quantitative information published on the conductivity of doped layers as a function of doping density and annealing temperature. Pavlov, Zorin, Tetel'baum, and Granitsyna [25], however, have published information on the mean conductivity of silicon doped by boron ions implanted at energies between 25 and 150 keV. This work does not include measurements of mobility of carriers in the implanted layers, so that it is not possible to derive the number of ions that become electrically active after heat-treatment.

In order to estimate the deviation from the doping activity calculated from the injected concentration, they define a quantity f (utilisation coefficient) such that $f = (n_p + N_i)/N_i$, where n_p is the mean carrier concentration (holes) in the doped layer, N_i is the mean concentration of boron atoms injected. The quantity f is then equal to unity in the equilibrium state (assuming that each boron atom injected is an ionised acceptor). Fig. 20 shows the values of f obtained for the range of doping densities and annealing temperatures together with the measured conductivity σ. It is seen that, at doses of 10 μC/cm^2, f is as high as 50% when the annealing temperature is only 600° C. When the dose is increased to 1000 μC/cm^2, it is then necessary to anneal at 800° C to produce 25% activity. The dependence of the mean conductivity of the doped layer on time is shown in fig. 21 for two values of annealing temperature, namely 300 and 700° C.

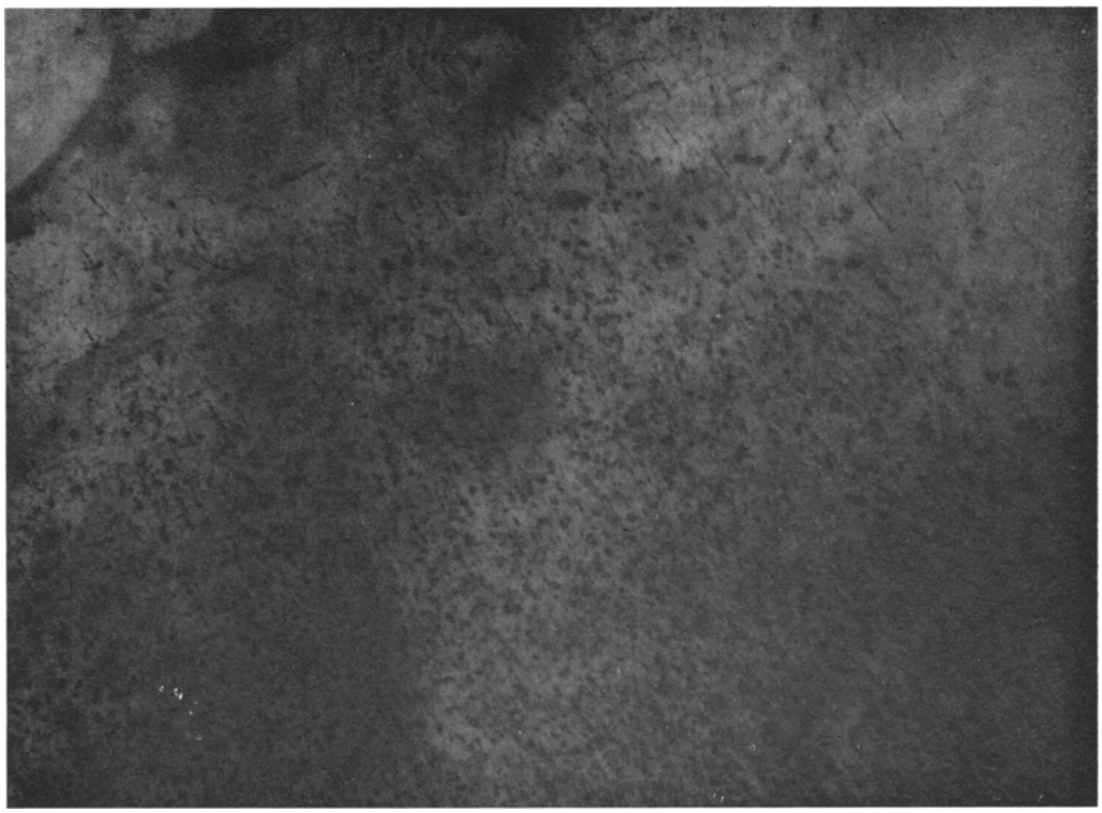

Figure 17a Heavily bombarded silicon (10^{16} boron ions/cm^2) before thickness reduction by anodiation and etching ($\times$ 46 000).

7. Experimental Profiles

One of the most useful aspects of ion-implantation doping of semiconductors is the high degree of control of profiles which is potentially possible. Fig. 22 shows examples of profiles that should be possible by suitable programming of the beam voltage. The extent to which these theoretical distributions can be obtained in practice is the object of a considerable amount of work at present. An example of a very shallow junction is shown in fig. 23; it was produced at SERL by the bombardment of germanium by 100 keV antimony ions [23]. Here, a divergent beam was incident on a (1 1 1) face and the doping produced is essentially that predicted for an amorphous solid, although a small proportion of ions may have channelled but these are not detected electrically. The junction depth of ~ 0.18 μm could be reduced by a lower beam energy, and shallow junctions of this type would be difficult to produce controlably by diffusion. Fig. 24 shows an example of a buried layer of p-type silicon produced by implanting boron ions into silicon at 100 keV energy [26]. Once again, the profile was measured by successively etching-off uniform layers of silicon and measuring the sheet conductivity using four-point probes and it is in close agreement with that predicted theoretically for amorphous silicon. The single crystal was mounted such that a (1 1 1) face was 8° from the direction normal to the ion beam and the maximum doping level was only 2×10^{18}/cm^3. As the velocity of the incident boron ions is reduced, the acceptance angle for channelling increases and it is possible to detect, electrically, a small proportion of channelled ions. A more sensitive method of studying the distribution of doping atoms is to use radioactive ions and measure their activity after successively stripping-off layers of crystal, although this gives no indication of their electrical activity. Gibbons, El-Hoshy, Manchester, and Vogel [27] have carried out such measurements for 40 keV phosphorus ions incident on a (1 1 1) face of

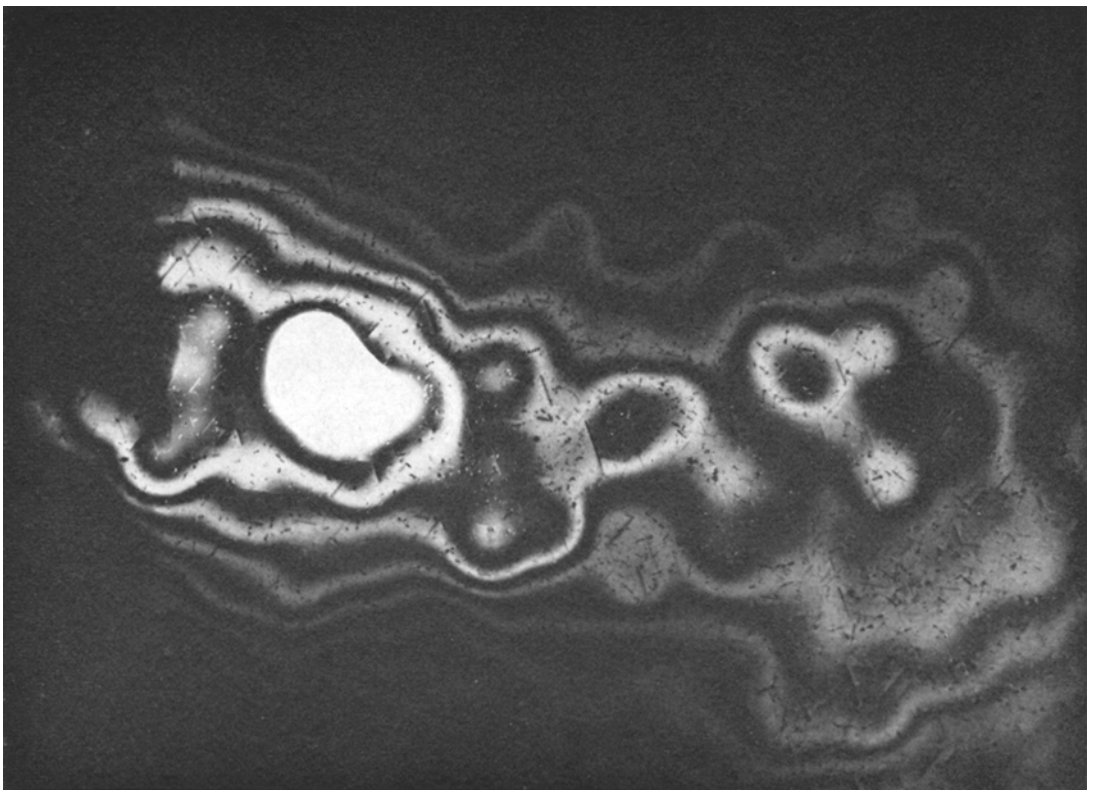

Figure 17b The same specimen as in fig. 17a, anodised and etched fourteen times at 100 V. The dislocation loops have disappeared and the ends of many of the long straight dislocations are still visible. The estimated thickness reduction is about 15 000 Å (× 46 000).

silicon. Fig. 25 shows the distribution obtained when radioactive P^{32} ions were incident at this energy and when the crystal was subsequently stripped. Fig. 26 shows the distribution obtained when $5 \times 10^{14}/cm^2$ of P^{31} ions were incident before injecting the P^{32} ions. The P^{31} ions damage the crystal so that channels are blocked and ions that do find their way into channels are not detected by the measuring technique. When the P^{32} ions are then incident on the crystal, it appears much like an amorphous solid and very little channelling takes place. The profile is then Gaussian and agrees very closely with that predicted by Lindhard *et al* [8].

In the production of p-n junctions in semiconductors, the technique has advanced to a stage where junction depths can be controlled very well, although it must be stressed that the technique is only suitable for the production of relatively shallow junctions. With a beam energy of 150 keV, it is possible to produce junction depths ~ 1 μm in 1Ω cm material using light ions such as boron, and increasing the beam energy to 500 keV would only result in junctions approximately twice as deep. Channelling can be used, however, to produce deep junctions at relatively low energies, but it is not known as yet whether this method can be controlled sufficiently to be used in an industrial process.

8. Advantages and Applications of Ion Implantation in Semiconductor Doping

The use of ion beams in the doping of semiconductors could have wide applications. Diffusion of impurities into silicon is a very well-controlled process and is adequate for the majority of devices today, but, as these structures become more sophisticated and, in particular, more shallow, ion-implantation techniques should be of great use. In this field, it is likely that industry will use ion implantation in addition to diffusion for the special devices which can benefit from it. With compound semi-

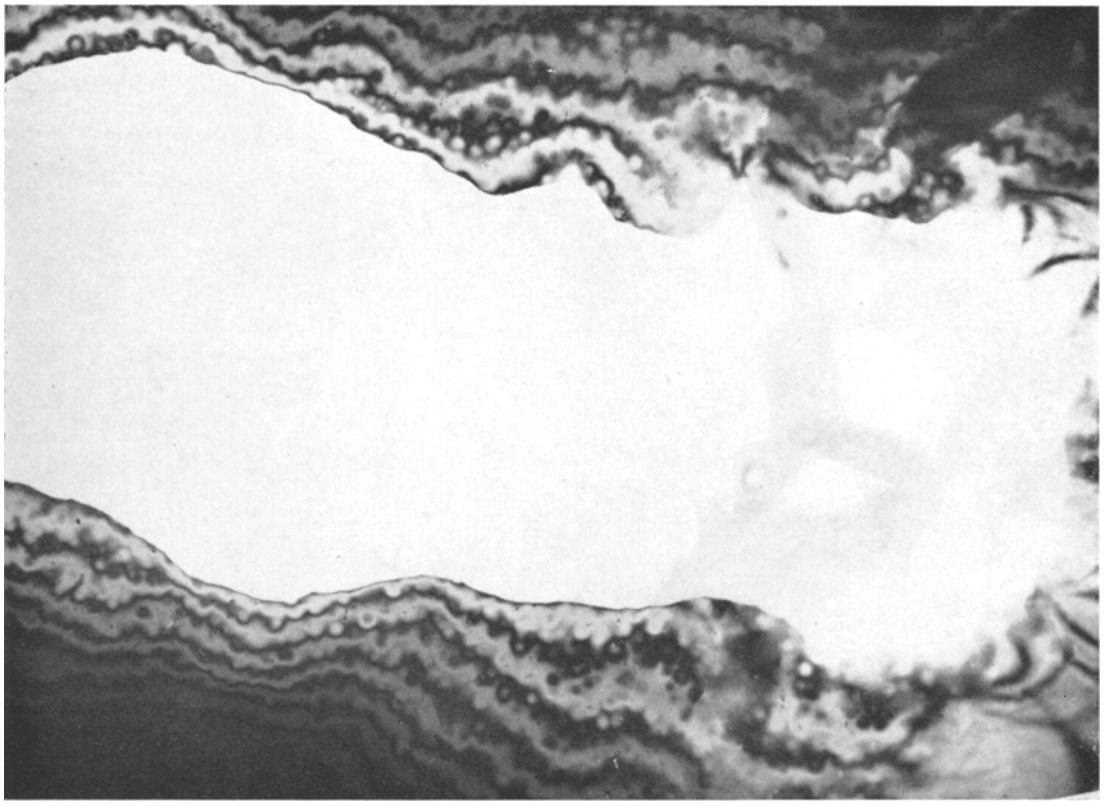

Figure 17c The same area as in fig. 17a, anodised and etched eighteen times at 100 V. There are few remaining defects of any sort left visible. The estimated thickness reduction is about 2500 Å* (× 46 000).

conductors, diffusion is much less controlled and sometimes cannot produce the conductivity required. Ion implantation would seem to be ideally suited for the doping of such compounds as gallium arsenide, zinc selenide, cadmium sulphide, silicon carbide, and many others.

In order to explore the use of this technique in device fabrication, there exists a programme at SERL and a cooperative programme between SERL and ASM Ltd† in which devices are produced which benefit from the particular advantages of ion implantation. Some of these advantages are listed below with reference to devices which receive benefit.

8.1. Control of the Doping Profile

The distribution of impurities in depth can be controlled to a high degree by programming the beam energy. This leads to advantages in the manufacture of, for example, high-frequency transistors. The basewidth is capable of control to better than 0.1 μm, and the sharp cut-off, possible because of the Gaussian distribution, leads to potential advantages in the base doping. Hybrid devices implanted at SERL and constructed by ASM Ltd have shown high gain when the emitter is implanted and the base diffused and, at this stage, doping profiles necessary for the base have been achieved. Other devices which benefit by the close control of doping profile are variable capacitance diodes and solar cells. The profile shown in fig. 23 has been used in producing large-area, shallow, germanium diodes which would be difficult to produce by diffusion. This demonstration of the production of large-area, shallow junctions could be very important in the manufacture of shallow silicon devices normally easy to produce in small areas but much more difficult to control over larger areas.

*The anodisations in this experiment have subsequently been shown to have been incomplete. Normally 12 anodisations at 100 volts are sufficient to remove 2500 Å silicon.

†Associated Semiconductor Manufacturers Ltd, Hirst Research Centre, Wembley, Middx, UK.

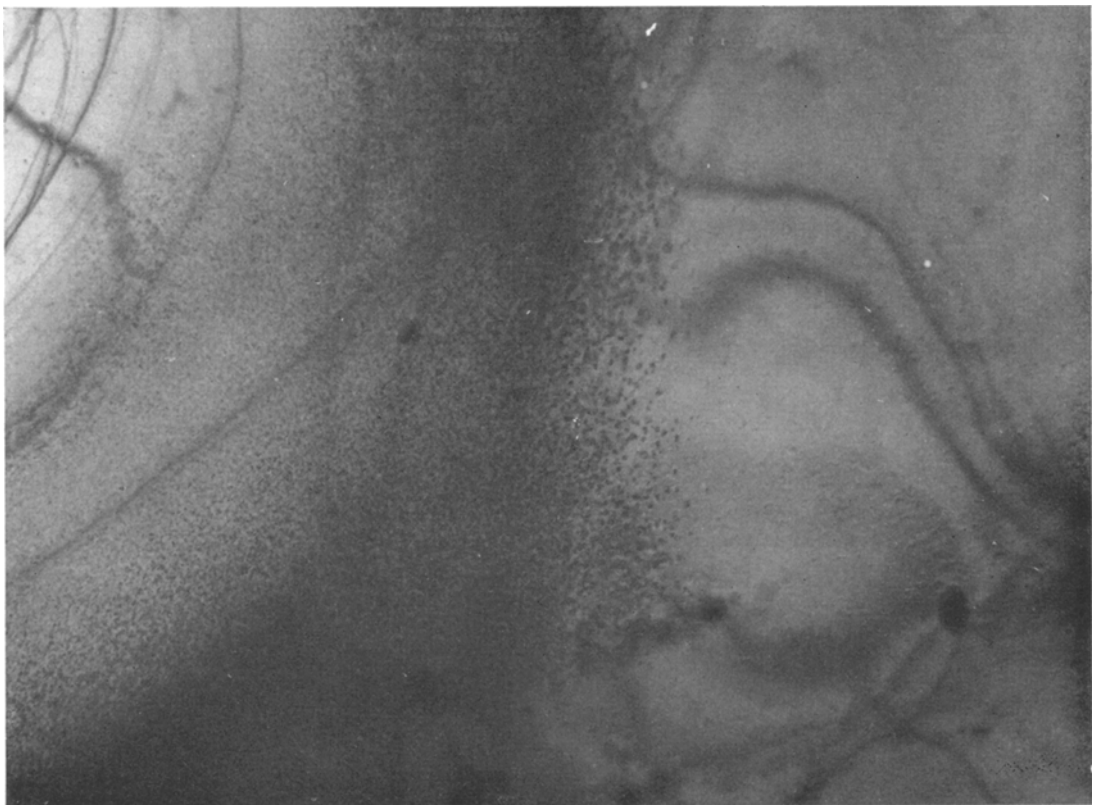

Figure 18 Bombarded silicon (4×10^{15} boron ions/cm^2) after annealing. There are no defects in the very thin area near the edge of the etch pit ($\times$ 46 000).

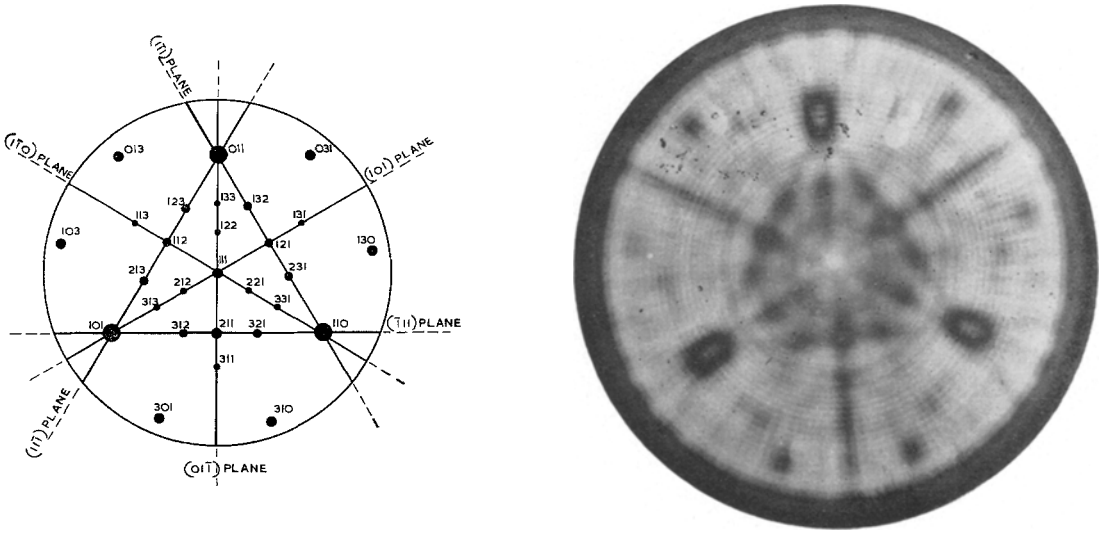

(a) (b)

Figure 19 (a) The radial projection of the directions about the 1 1 1 pole of silicon indexing the easy channelling directions as seen in (b). (b) A photograph of an ion-bombarded (1 1 1) silicon slice. The milky areas are amorphous and the dark areas are the easy channelling directions.

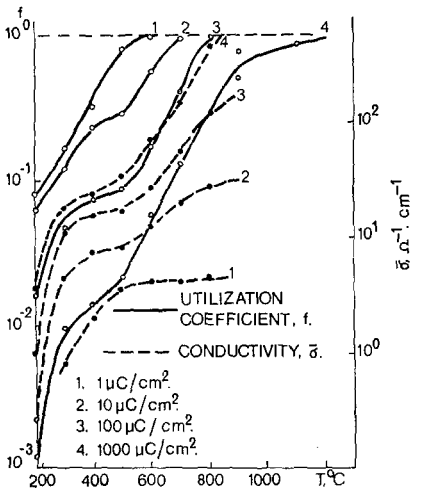

Figure 20 Dependence of the mean conductivity of the inversion layer and utilisation coefficient on annealing temperature. Annealing time 30 min.

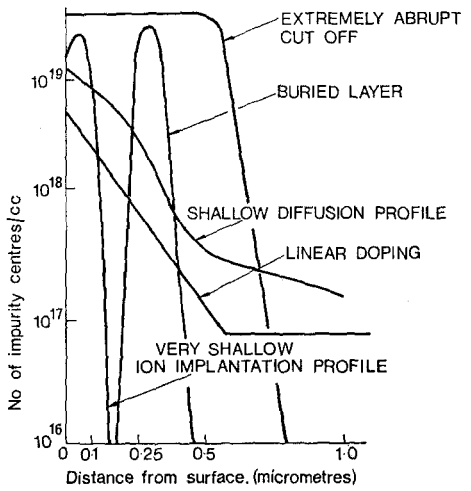

Figure 22 Profiles possible by ion implantation.

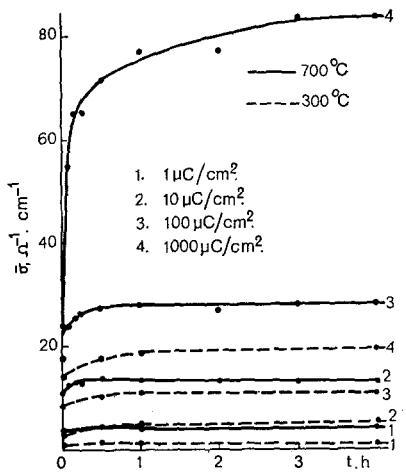

Figure 21 Dependence of the mean conductivity of the inversion layer on annealing time.

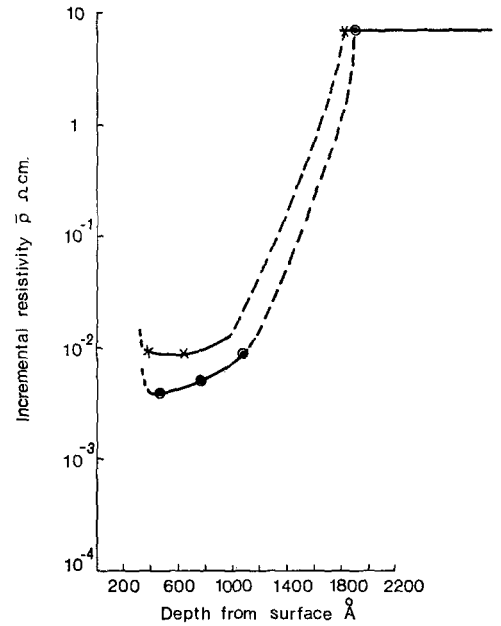

Figure 23 Shallow junctions in Ge by 100 keV Sb^+ implantation.

8.2. Low-Temperature Nature of the Process

This leads to the possibility of producing p-n junctions in compounds which normally exhibit auto-compensation whereby carriers of a particular type introduced are automatically compensated by crystal defects of the opposite type. This occurs, for instance, when zinc selenide or cadmium sulphide are doped by conventional techniques by impurities that should produce p-type conductivity. By implanting the impurities at much lower temperatures, it may be possible to avoid this effect and produce high-conductivity p-type regions in these II-VI compounds. At SERL, it has been shown that high-resistivity n-type zinc selenide has been rendered conducting by implanting impurities, but, as yet, various material problems such as the difficulty of making shallow contacts have prevented proper electrical characterisation of the implanted layers.

The use of ion beams with mass analysis provides a way of introducing only the impurities

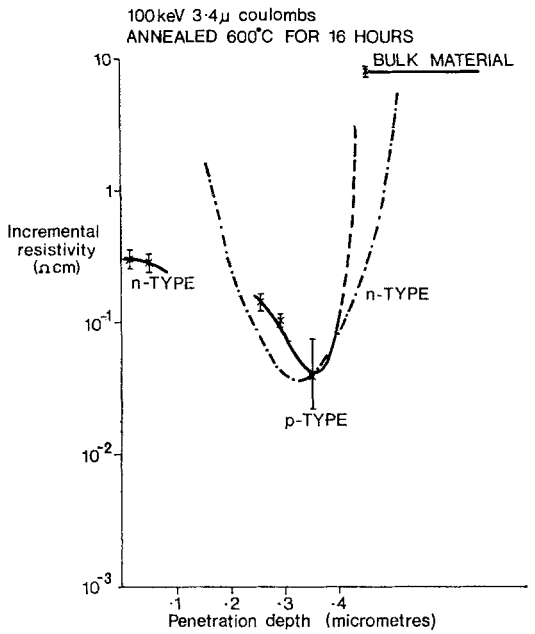

Figure 24 Buried layer formation at 100 keV. Annealed at 600° C for 16 h.

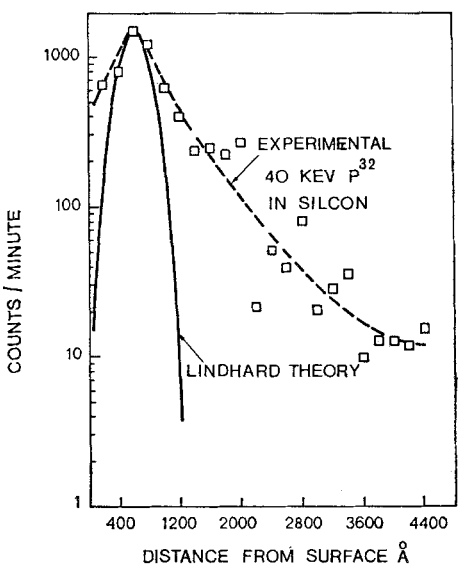

Figure 25 Concentration profiles for 40 keV P^{32} ions incident on single crystal silicon compared with theoretical profile for an amorphous silicon target.

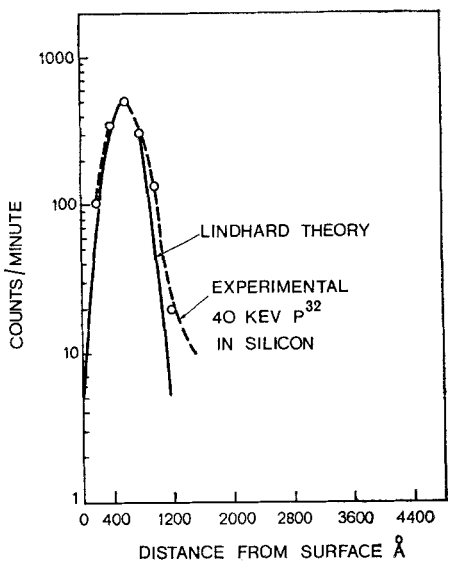

Figure 26 Concentration for 40 keV P^{32} ions after first implanting $5 \times 10^{14}/cm^2$ of P^{31} ions in the single crystal target.

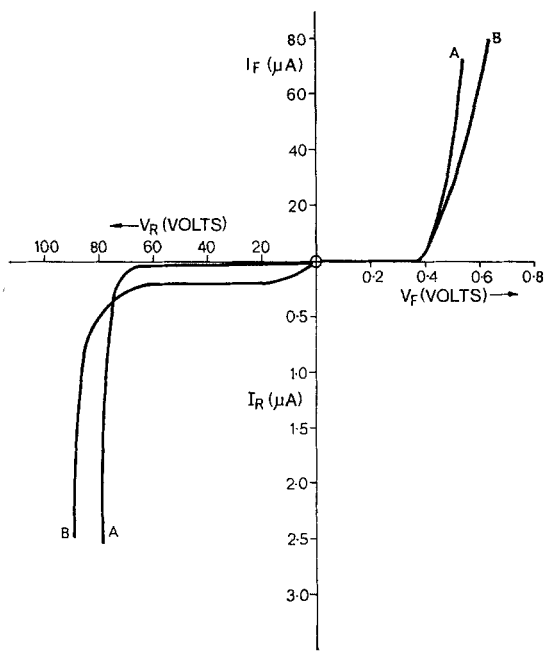

Figure 27 Typical *I-V* characteristics of ion implanted mesa diodes.

required rather than unwanted ones which can be introduced by high-temperature processes such as diffusion. Fig. 27 is the electrical characteristic of a phosphorous-doped silicon mesa diode of area 6.25×10^{-4} cm². The annealing temperature of such diodes can be as low as 600° C and the resulting reverse characteristic of many such diodes suggest that there are no microplasmas,

possibly owing to the low-temperature nature of the process. The effective lifetime of diodes such as this has been shown to be at least as good as similar diffused diodes, and presumably the lifetime of the bulk material is less degraded by the low-temperature nature of the process. This aspect has potential advantages in the design of detectors and solar cells.

One of the causes of device failures is the anomalous penetration of impurities by diffusion at points in the crystal where the lattice is imperfect, such as a dislocation. The penetration of an ion will be much less affected by such imperfections and, provided the annealing temperature is low, the chances of anomalous penetration by diffusion should be much reduced. This may be important when large-scale integration is carried out in microcircuits.

8.3. Low Lateral Spread

The directional properties of ions penetrating a crystal are such that there is every reason to expect that the spread of impurities through a hole in a mask should be much less than by diffusion, which is essentially a three-dimensional process. This is important when device structures become so small that registration becomes difficult in photolithographic processes. For example, the considerable research into exposure of photoresist by electron beams to produce very small, accurately registered areas could be exploited by then introducing impurities by ion beams. Already, gate masking of the ion beam has been tried in the USA in the manufacture of a MOST*. This produces the source and drain regions accurately aligned with respect to the gate and with much reduced overlap.

8.4. Introduction of Insoluble Impurities

Impurities can be forced into crystals in which they are not normally chemically soluble. This affords a means of producing supersaturated solutions of an impurity in the host material which may produce interesting electrical properties. An example is the doping of diamond which usually occurs naturally as an insulator or a slightly n-type conductor. Diffusion doping of diamond involves the application of high temperatures and pressures. Wentorf and Darrow [28] have shown that the injection of nitrogen in the form of ions causes the diamond to become more n-type. More recently, Vavilov *et al* [29] have doped diamonds both p- and n-type by using boron and lithium ions respectively. The degree of conduction produced by high ion concentrations was 5 to 10 orders of magnitude greater than before irradiation.

8.5. Beam Methods for Producing Microcircuits

The possibility of producing doped regions on a semiconductor by "writing" with a beam of ions was postulated by Shockley [30]. Conventional masking of diffusion is obtained by using oxide layers that are delineated by using photolithographic processes. Using a focused beam, it may be possible to produce arrays of devices by deflecting the beam in the required fashion, possibly controlled by a computer. A combination of ion beams and electron beams could provide an all-vacuum method for producing microcircuits which would preclude the need for lengthy photolithographic processes. Much more information is needed on such aspects as limiting beam size, stability, and writing speed, before such a process can be considered viable, and the economics of such a technique are difficult to evaluate without this information. Considering only the ion beams, however, calculations of space-charge spreading of the beam show that micrometre sizes are theoretically possible. Alternatively, oxide masking produced by electron beam techniques could be used in conjunction with "flood" ion beams. Simple calculations show that the magnitude of beam current density that can be tolerated in micrometre dimensions is limited by the heating effect caused by such a beam. However, using 100 μsec pulses of 100 keV ions, it should be possible to dope a 1 μm cube volume to a concentration of 10^{20} carriers/cm^3 in a total time of 0.01 sec or 100 pulses. Larger areas could be doped in similar times by increasing the current density proportionately. Such a process would be particularly suitable for very complex circuits in which a high packaging density of very small components is required with good registration.

References

1. R. S. OHL, *Bell Syst. Tech. J.* **31** (1952) 104.
2. W. D. CUSSINS, *Proc. Phys. Soc.* **68** (1955) 213.
3. F. M. ROURKE, J. C. SHEFFIELD, and F. A. WHITE, *Rev. Sci. Instr.* **32** 455.
4. J. O. MCCALDIN and A. E. WIDMER, *J. Phys. Chem. Solids* **24** (1963) 1073.
5. R. R. FERBER, *Trans. IEEE Nucl Sci.* **NS10** (1963). 15.

*metal/oxide/semiconductor transistor

6. W. J. KING, Proc 4th Photovoltaic Specialists Conference, Chicago (1964)
7. N. BOHR, *Math-fys Medd.* **18** No. 8 (1948).
8. J. LINDHARD, M. SCHARFF, and H. E. SCHIOTT, *ibid* **33** No. 14 (1963).
9. J. A. DAVIES, J. D. MCINTYRE, R. L. CUSHING, and M. LOUNSBURY, *Canad. J. Chem.* **38** (1960) 1535.
10. G. R. PIERCY, F. BROWN, J. A. DAVIES, and M. MCCARGO, *Phys. Rev. Lett.* **10** (1963) 399.
11. M. T. ROBINSON and O. S. OEN, *Appl. Phys. Lett.* **2** (1963) 30.
12. G. DEARNALEY (UKAERE, Harwell, Berks), private communication.
13. J. R. PARSONS, *Phil. Mag.* **12** (1965) 1159.
14. V. F. GIANOLA, *J. Appl. Phys.* **28** (1957) 868.
15. G. R. BOOKER and R. STICKLER, *Brit. J. Appl. Phys.* **13** (1962) 446.
16. A. HOWIE and M. J. WHELAN, *Proc. Roy. Soc.* **267** (1962) 206.
17. D. J. MAZEY, R. S. BARNES, and R. S. NELSON, Proc. of the 6th International Congress for Electron Microscope, Kyoto, 1966 (Maruzen, Tokyo, 1966), p. 363.
18. H. P. KLUG and L. E. ALEXANDER, "X-ray Diffraction Procedures" (Wiley, 1954), pp. 586-620.
19. H. VON RICHTER and G. BREITLING, *Z. Naturforsch.* **13a** (1958) 988.
20. W. L. BELL and G. THOMAS, *Phil. Mag.* **13** (1966) 395.
21. P. B. HIRSCH, A. HOWIE, R. B. NICHOLSON, D. W. PASHLEY, and M. J. WHELAN, "Electron Microscope of Thin Crystals" (Butterworths, 1965), pp. 1-23.
22. M. F. ASHBY and L. M. BROWN, *Phil. Mag.* **8** (1963) 1649.
23. L. N. LARGE and H. HILL, Proc. of the 2nd International Conference on Electron and Ion Beam Science and Technology, New York, 1966 (Wiley, in press).
24. R. S. NELSON, D. J. MAZEY, M. D. MATTHEWS, and D. F. HOLLOWAY, *Phys. Lett.* **23** (1966) 18.
25. P. V. PAVLOV, E. I. ZORIN, D. I. TETEL'BAUM, and E. K. GRANITSYNA, *Fiz. Tverdoge Tela.* **7** (1965) 2940 (translation: *Soviet Phys. Solid State* **7** (1966) 2386).
26. L. N. LARGE, H. HILL, and M. P. BALL, *Int. J. Electronics*, **22** (1967) 153
27. J. F. GIBBONS, A. EL-HOSHY, K. E. MANCHESTER, and F. L. VOGEL, *Appl. Phys. Lett.* **8** (1966) 46.
28. R. H. WENTORF and K. A. DARROW, *Phys. Rev.* **137** (1965) 1614.
29. V. S. VAVILOV, M. I. GUSEVA, E. A. KONOROVA, V. V. KRASNOPEVTSEV, V. F. SERGIENKO, and V. V. TUTOV, *Fiz. Tverdogo Tela (USSR)* **8** (1966) 64.
30. W. SHOCKLEY, US Patent No. 2 787, 564 (1957).

Letter

Anisotropy in the Shear Modulus of Glassy Polymers

Robertson and Joynson [1] have studied the stress/strain properties of some uniaxially drawn, glassy polymeric films, in simple shear, as a function of the angle (θ) between the direction perpendicular to the shear and the orientation axis of the material. The sense of the angle θ is indicated in fig. 1. The materials studied were uniaxially drawn poly(2,6-dimethylphenylene oxide) and poly(4,4′-dioxydiphenyl-2,2-propane carbonate) with draw ratios 1.65 and 1.46 respectively. For both materials, it was observed that the shear stress, at a total shear strain of 4/3, passed through a pronounced maximum at θ between 55 and 60° and a less pronounced minimum at θ between 145 and 150°.

Similar studies have now been made on uniaxially drawn amorphous poly(ethylene terephthalate) film with a draw ratio of 5. The apparatus used was similar to that described by Robertson and Joynson [1], having two clamps separated by 0.0195 cm constrained to move parallel to one another by low-friction linear bearings, and could be attached to an Instron tensile testing machine for measurements of force and displacement.

The initial shear moduli of the film in different directions could not be measured accurately because of the impossibility of clamping the film so that it was completely flat, the stress/strain curve having therefore a curved toe. There were, however, two approximately equal maxima when θ was equal to 45 or 135°. Such a result is to be expected. After drawing, the increase in the tensile modulus in the draw direction is much greater than the reduction in the tensile modulus in the perpendicular direction. Since, for small strains, shear is equivalent